



Blast mitigation by water mist: the effect of the detonation configuration

T. Schunck¹ · M. Bastide¹ · D. Eckenfels¹ · J.-F. Legendre¹

Received: 29 April 2019 / Revised: 27 February 2020 / Accepted: 12 July 2020 / Published online: 7 September 2020
© Springer-Verlag GmbH Germany, part of Springer Nature 2020

Abstract

In this paper, blast mitigation using water mist was evaluated to assess the operational capability of the use of firefighting systems implemented in ships or infrastructures to reduce blast effects. In particular, we tried to determine the mitigation that could be obtained in specific situations. A tunnel equipped with a water mist system enabled us to assess the mitigation impact of water mist on a blast. Blast effects were evaluated using four pressure gauges on the tunnel walls and one pressure gauge at the end of the tunnel. As a first step, we evaluated the mitigation efficiency based on water mist characteristics (the droplet size and the water load) when the charge was detonated inside the mist, the tunnel being either open or closed. Then, we assessed the mitigation efficiency when the charge was detonated outside the mist with only the blast wave propagated in the mist. The reduction in the initial overpressure and the maximum impulse were higher when the charge exploded inside the water mist, and this is most likely due to the quenching of secondary reactions by the water mist. To obtain a better understanding of mitigation mechanisms, shock tube experiments were conducted. The break-up of water drops in the high-speed airstream behind the shock wave was observed, but the presence of mist had no significant effect on the shock wave profile. This is in line with the importance of fireball extinguishment in the mitigation process.

Keywords Blast · Mitigation · Water mist

1 Introduction

It is a well-known fact that explosion effects can be significantly mitigated if a detonating charge is surrounded by a layer of water. Water can be used in various physical forms. This includes bulk water [1–4], water spray or mist [5–16], and water-based foams [17, 18]. Water mist mitigation concepts can be used to good advantage in the design and operation of new and existing facilities exposed to the threat of an internal explosion, for instance ammunition storage sites or ships. It is also suitable for sensitive facilities, e.g., for

the protection against terrorist bombings. In the case of a confined explosion, water mist has the potential to attenuate both the shock pressure and the gas pressure loading developed inside the structure. The water mist system would be activated preventively if there was an imminent risk of detonation.

While some studies describe the mitigation of dust, hydrocarbon mist, and vapour/gas cloud explosions using water mist [5, 8], a certain number of studies focus on the use of water mist to mitigate the blast effect of a high explosive [9–16]. One of the previously published studies was carried out in free field [14] in which the charge exploded outside the water mist. The water mist curtain was generated by seven nozzles positioned 50 cm apart delivering a water flow rate of 3 litres per min (lpm). The Sauter mean diameter, SMD, (diameter of the droplet whose surface-to-volume ratio is equal to that of the entire spray) of the droplets was about 100 μm , and the water mass fraction was estimated at about 50 g/m^3 . Seven pressure gauges were used: two were located inside the mist, two behind the mist curtain and two placed at the same distance as the latter ones but symmetrical to the charge position. It appeared that in

Communicated by D. Frost.

Electronic supplementary material The online version of this article (<https://doi.org/10.1007/s00193-020-00960-1>) contains supplementary material, which is available to authorized users.

✉ T. Schunck
therese.schunck@isl.eu

¹ ISL, French-German Research Institute of Saint Louis, 5 rue du General Cassagnou, BP 70034, 68301 Saint Louis Cedex, France

that case, the overpressure generated by 4.5 kg of Plastrite (87% PETN, 9.75% NYTEX oil, 3.25% binder) was only lowered inside the mist (44%), but was not impacted after passing through it. The other studies published were conducted in a closed facility [9–13, 15, 16]. Resnyansky and Delaney [10] assessed the mitigation of blast wave produced by charges of 500 g of Composition B with a mist generated above the charge. They obtained a reduction of 10% in overpressure. They also tested a configuration in which the mist was generated by a line of nozzles positioned behind the charge and the pressure gauges were located inside the mist. In that case, the overpressure was decreased by 20%. A series of experiments were conducted with TNT charges of 0.9, 2.2, and 3.2 kg [9] and six nozzles producing the mist. It has been shown that the maximal overpressure was reduced in all tests as well as the quasi-static overpressure. Willauer et al. [11] assessed the water mist mitigation of the blast generated by 22.7 kg of TNT and by a Destex charge with the same TNT equivalent. The impulse and initial blast wave overpressure for the TNT charge were reduced by 40% and 36%, respectively. For the Destex charge, the reduction in initial overpressure was lower (25%) but the reduction in impulse was equivalent (43%). The quasi-static overpressure reduction was similar for both charges, it ranged between 33 and 35%. Willauer et al. [12] also conducted experiments using 22.7 kg TNT equivalent of PBXN-109, and the impulse, initial blast wave, and quasi-static overpressure were reduced by 49%, 39%, and 41%, respectively. They also tested different conditions of mist (droplet size and concentration) with the three explosives (TNT, Destex, PBXN-109). They observed that blast mitigation was higher with high mist density, but the droplet size was different across the different mist densities. The same blast mitigation was obtained with high mist densities (70–90 g/m³) and different SMDs (54 and 84 µm). Mataradze et al. [15] assessed the water mist mitigation of the blast generated by 10 g of RDX that exploded outside the mist. Three water loads were tested: 5.1 g/m³, 19.8 g/m³, and 36.6 g/m³, and the overpressure was reduced by 22%, 47%, and 53%, respectively. The droplet size was between 25 and 400 µm.

Overall, in the previously published studies, it has been shown that the overpressure, the impulse, and the quasi-static pressure of an explosion were all reduced by the presence of mist. However, the blast wave reduction was spread over a rather broad range. Previous studies [7–9, 13] assumed that droplet size and water load were the factors that most influenced explosion attenuation. From these studies, it was difficult to evaluate the mitigation efficiency according to the type of water mist, as the characteristics of the mists differed significantly. Moreover, most of the time, only one sort of water mist was tested, and the water mist was not always characterised precisely. The water load

was only estimated, probably from the water flow, and the estimation method was not given. The study [11, 12] that did measure properly mist concentration and droplet size used a laser light scattering analyser. The analyser provided the droplet size distribution and mass loading measurements as a function of time. They mapped the concentration and droplet size in the chamber at three separate locations and two different heights at those locations.

In addition, the previous studies did not clearly show whether the difference in blast mitigation occurred because the charge detonated in the mist or not. When the charge detonated outside the mist, Tosello et al. [14] observed no blast attenuation behind the mist, but Resnyansky and Delaney [10] obtained a better attenuation compared to the case of a detonation inside the mist. Mataradze et al. [15] registered a reduction of up to 53%, whereas Resnyansky and Delaney [10] registered a reduction of only 20%.

Concerning the mechanisms leading to blast mitigation by water mist, it was initially suggested that convective and radiative energy transfers were an important part of energy absorption. Afterwards, other mechanisms were added: the withdrawal of kinetic energy, the extraction of energy for droplet vaporisation, and the quenching of secondary reactions [19]. Thomas [7] stated that the controlling physical mechanism is the relative acceleration of droplets compared to the accelerating gas flow; thus, large droplets (> 1 mm) with large inertia could be more effective than small droplets. Using numerical modelling, it was also shown [4] that the absorption of the latent heat of vaporisation is the dominant mechanism of energy absorption and thus, small droplets could contribute more effectively to the energy extraction from the blast as their vaporisation duration is shorter. However, large droplets could fragment and although the fragmentation energy is low compared to the vaporisation energy of water, the fragmentation could be necessary for the global process. Small droplets are generated and these could evaporate rapidly.

The French-German Research Institute of Saint-Louis has therefore developed a facility and a method to evaluate the mitigation properties of water mist and its characteristics. A tunnel was built and equipped with a water mist fire suppression system. The water mist generation system comprised a high-pressure pump and eight nozzles. To test different droplet sizes, nozzles generating “small” droplets and nozzles generating “large” droplets were used. An effort was made to characterise properly the water mist. The method chosen to estimate the water concentration of the different mists was to use the water distribution on the floor and the time of flight (TOF) of the droplets from top to bottom in the tunnel. In this work, three detonation scenarios were investigated: either the charge was placed in the centre of the tunnel and consequently detonated inside the mist, the tunnel was either open or closed, or the charge was detonated

in front of the tunnel 4 m from the entrance so only the shock wave travelled through the mist. The water mist's effect on blast wave overpressure and impulse loading generated by the detonation of Composition B spheres was assessed. As part of this research, and in addition to real-size experiments, shock tube studies were carried out to obtain a better understanding of blast mitigation mechanisms. Therefore, the break-up of water drops in the high-speed airstream behind a shock wave in a shock tube was investigated. The break-up of water drops by a shock wave at a Mach number of around 1.3 was recorded using a high-speed camera. The shock wave profile used in the shock tube corresponds to a blast wave. The effects of the water drop break-up on shock pressure were also assessed.

2 Experimental set-up

2.1 Facility

The tunnel was 4.35 m long, 2 m wide, and 2.8 m high. The tunnel was equipped with a water mist fire suppression system consisting of a high-pressure pump (SEM-SAFE[®], Danfoss, Semco, 114 litres per minute (lpm), 120 bar) and nozzles. Three types of nozzles were used. The first and the second types (F500.147.37.04 and F500.143.37.04, DEF “Département Risques Spéciaux”, France) generate small droplets (diameter of about 25–100 μm), and the third type (17 90 05, DEF “Département Risques Spéciaux”, France) generates large droplets (diameter of about 200–300 μm). In the following text, F500.147.37.04 nozzles are named as “147,” F500.143.37.04 nozzles are named as “143,” and 17 90 05 nozzles are named as “17.” Three detonation scenarios were investigated: either the charge was placed in the centre of the tunnel and therefore detonated inside the mist, with the tunnel being either closed or open, or the charge was detonated in front of the tunnel, 4 m from the entrance (Fig. 1).

The three detonation scenarios were tested with the small-droplet nozzles and the large-droplet nozzles. Eight nozzles were used to produce the mist. They were divided into two rows of four nozzles at a distance of 0.7 m apart. Each row was placed 0.65 m from one tunnel wall. The nozzles were 1.1250 m apart. The first nozzle in the first row was placed 0.2812 m from the tunnel entrance, and the first nozzle in the second row was placed 0.8437 m from the tunnel entrance.

As the DEF “Département Risques Spéciaux” has stopped manufacturing “147” nozzles, it was only possible to obtain six nozzles of this type. We therefore used two types of nozzles to produce small droplets. As our research concerned an eight-nozzle set-up, the series was completed with two “143” nozzles. In supplementary Table 1, the geometric characteristics of the nozzle are given.

2.2 Metrology of water mist characteristics

The flow from each nozzle was determined by collecting the entire ejected mass of water in a plastic barrel over a given period of time. The mean was determined from four measurements carried out for each nozzle.

Concerning the water concentration of the mists, it was initially envisaged to measure the droplet size distribution and the water load of the mist by laser diffraction measurements, but unfortunately, the results were not satisfying. First, the outdoor brightness depending on the weather conditions interfered with the calibration of the device (measurement of the diffracted light background). Secondly, the mists used were very dense and the particle size analyser was rapidly saturated. In order to limit the effect of outdoor brightness and prevent a massive influx of droplets into the measuring head, a cover perforated with two round holes was placed on this head. Consequently, it was only possible to measure the droplet size distribution. For the nozzles ejecting the “small” droplets, measurements were realised at different positions in the tunnel, and exploitable results were

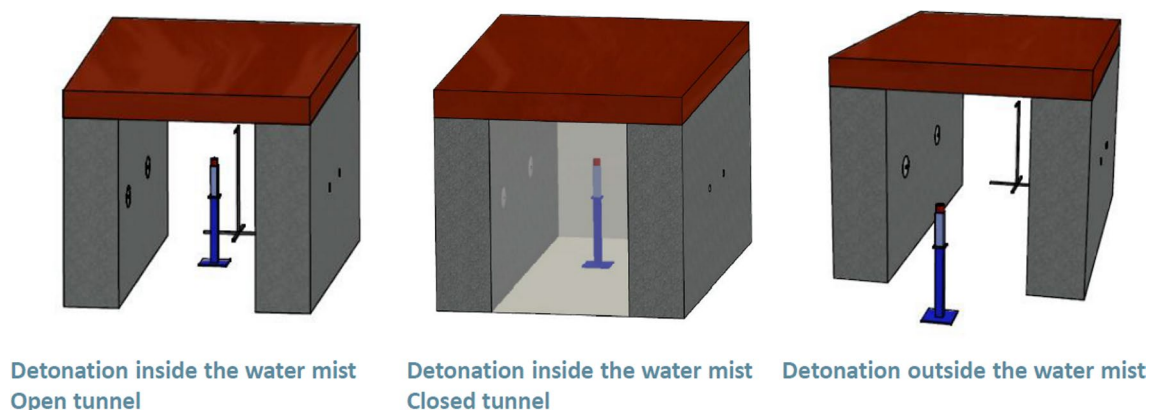


Fig. 1 Detonation scenarios

only obtained on the extremities of the tunnel and closed to the walls where the water mist was the less dense. Inside the tunnel, below the nozzles, the particle size analyser was rapidly saturated. It could not be excluded that these measurements of droplet size distribution were biased as the cap placed on the measure head prevents the entering of droplets that fly less. Consequently, only the distribution of very small droplets was measured. For the nozzles ejecting large droplets, it was not possible to measure the particle size distribution. Either no droplets were detected in the measuring head or too many droplets entered the measuring head and clung to the optical windows of the latter, thus preventing the measurements. Therefore, the method used to estimate the water concentration of the mists was to use the water distribution on the floor and the TOF of the droplets from top to bottom in the tunnel. The water distribution on the floor was measured thanks to an array of 100 mm × 100 mm plastic boxes that collected water for a certain length of time.

2.3 Charges and blast measurements

The charges used for the detonation tests were homogeneous spherical charges of Composition B. The sphere mass was 57 g for the detonation inside the tunnel and 2.5 kg for the detonation in front of the tunnel. They were ignited at the centre by means of a high-voltage cap (RP 83) and a booster charge of C4, either 5 g for the small spheres or 110 g for the large spheres. The blast effects were evaluated using four reflected pressure gauges (PCB 113B28)

placed on the tunnel walls and one side-on pressure gauge (PCB 137 A 23) placed at the end of the tunnel. The exact position of the sensors and the charge for the detonation inside the tunnel is shown in Fig. 2, left. For the detonation in front of the tunnel, the charge was placed 4 m from the entrance (Fig. 2, right). It could be noted that contrary to the test where the charge detonated inside the tunnel and for which the angle of incidence was close to 15°, in that case, the angle was closer to 80°. Based on the regular reflection theory, the reflected wave can practically be assimilated to an incident wave.

The explosion test matrix is provided in Table 1.

Table 1 Explosion test matrix

Configuration	Detonation location	Droplet size	Number of tests
Open tunnel	Inside	–	6
Open tunnel	Inside	Small	8
Open tunnel	Inside	Large	7
Closed tunnel	Inside	–	3
Closed tunnel	Inside	Small	3
Closed tunnel	Inside	Large	3
Open tunnel	Closed	–	6
Open tunnel	Closed	Small	3
Open tunnel	Closed	Large	6

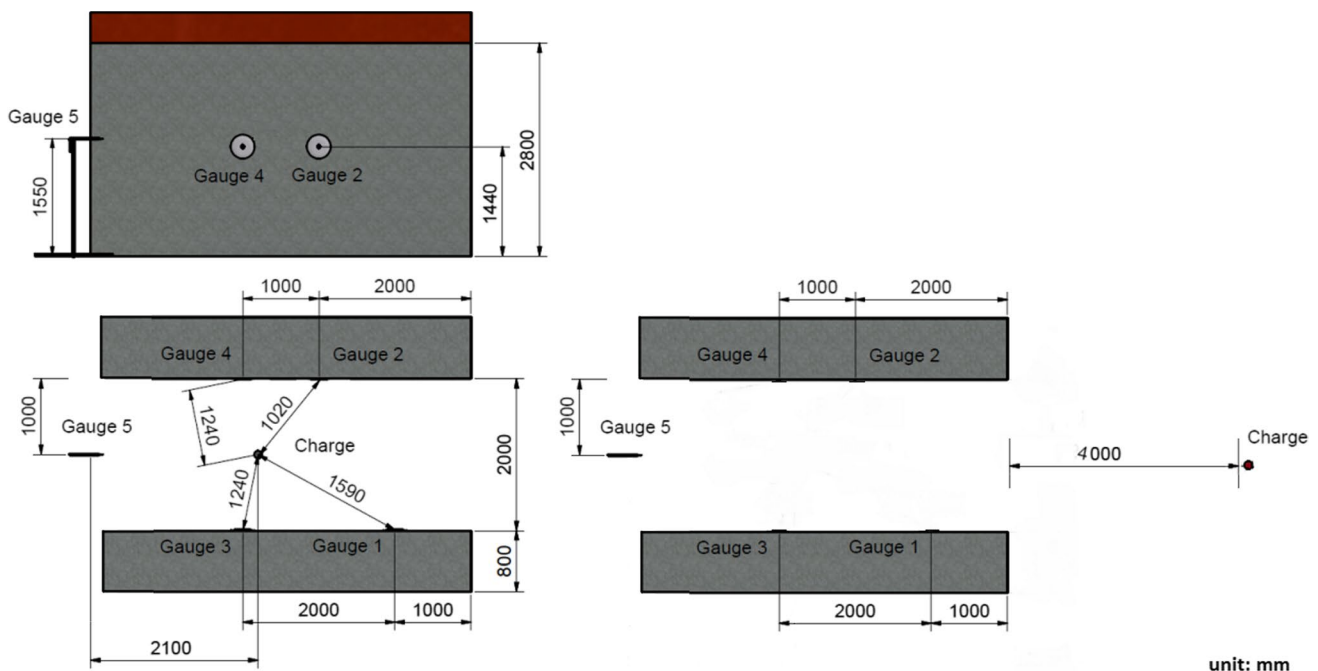


Fig. 2 Gauge positions inside the tunnel and charge positions with respect to the gauges

2.4 Shock tube experiments

We used a transonic shock tube which allows the generation of a blast shock wave known as the Friedlander wave. The shock tube comprised four sections: the driver section at high pressure (400 mm in diameter, 500 mm long), the driven section at atmospheric pressure (400 mm in diameter, 6970 mm long), the measurement section, which was rectangular (40 mm × 120 mm) with 220 mm-long viewing windows, and the extension section after the measurement section (rectangular and 1120 mm long) (Fig. 3). To allow high-speed video recordings, windows were integrated in the measurement chamber. Two conjoined membranes of Mylar (thickness 350 and 200 μm) separated the driving and driven sections during the pressure rise. The measurement section was connected to the driven section by means of a “cookie-cutter.” This device “cuts” the surface of the incident shock to properly reshape the circular incident wave into a rectangular one. It is placed 750 mm upstream from the test section inside the driven tube. The extension section was connected to the test section and prevented the reflections at the end of the tube from interfering too early with the pressure signals recorded in the test section. The shock tube was designed so that the reflection of expansion waves on the driver end could combine with the incident wave and the pressure signal in the tube at a certain distance from the membranes is similar to a blast shock wave. The experiments were conducted under the following conditions: pressure of 5 bars in the driver section and 1 bar in the driven section. A shock wave generated with a Mach number of 1.3 and incident pressure of 2 bars. Two PCB pressure gauges located 1705 mm (Piezotronics 113A21 model) and 3710 mm (Piezotronics 112A21 model) upstream from the beginning of the driven section recorded the overpressure profile. The shock velocity was obtained using the shock wave arrival time obtained by these gauges.

We achieved direct visualisation with a focus on the droplets using a Photron SA X high-speed camera with a maximum sensor size of 1024×1024 and a speed of 12,500 images/s. We reduced the region of interest (ROI) to enhance the frame rate, so that we could record several images where the shock wave front was visible in the measurement chamber. The imaging lens was decoupled from the camera body

and chosen based on the field we needed to observe and the desired magnification level. For all experiments, the chosen source was a 100 W halogen horizontal filament lamp. The goal of the experimental device was to fully illuminate the measurement chamber windows with parallel light. For this purpose, two convergent doublets were used to build an afocal system and illuminate a parabolic mirror. The image magnification on the camera sensor depends on the camera’s electronic magnification and on the ratio between the imaging lens and the mirror focal length. For a given camera, higher magnification can be obtained by decreasing the mirror focal length and/or by increasing the imaging lens focal length.

Two possibilities were investigated. First, the complete illumination system was left in place, and the second mirror was replaced by a 500 mm focal length doublet. In this case, the magnification gain was three, but the field was limited due to the small doublet diameter (65 mm). Then, we tried another set-up with a focal length of 1000 mm and a doublet diameter of 200 mm. The focal length of the imaging lens was also enhanced to 200 mm. In this case, the magnification was 0.2 and could reach 0.4 with a lens doubler added to the imaging lens. For this set-up, no more mirrors were required to illuminate the measurement chamber, the same doublet was used, and the set-up was used in an in-line way (Fig. 4).

The droplet generation system used for the break-up study consisted of an infusion reservoir, and the outlet of the infusion line was divided into several lines. Each line had a needle at its tip, and the needles were inserted in the upper plate of the test section. The water flow could be adjusted through the infusion bag system. In order to assess the effects of water droplets on the shock wave profile, experiments were also conducted with a water drop curtain. The system that generated the water drop curtain consisted of a small container machined directly into the viewing window ceiling and supplied with water by a small pump. The base of the container/viewing window ceiling was perforated (38 holes on a thickness of 70 mm) so droplets were generated and could fall into the measurement section. The water concentration was estimated thanks to the number of drops and the drop size in the water drop curtain: it was about 1.5 kg/m^3 . Two PCB surface pressure sensors (Piezotronics 112A21 model) were

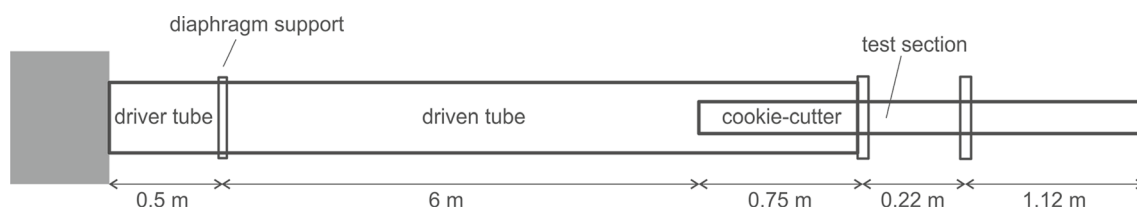


Fig. 3 ISL’s shock tube scheme with all dimensions in meters

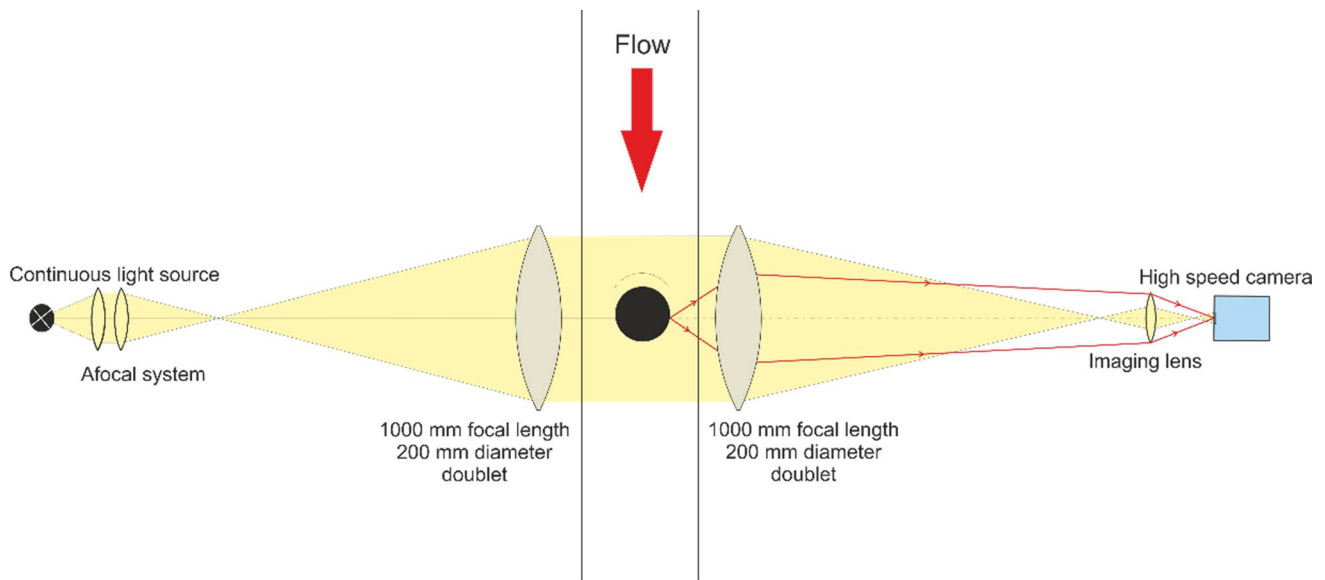


Fig. 4 Optical set-up for high-magnification direct visualisation

also placed 45 mm upstream and 45 mm downstream from the perforated area that the droplets came from in order to record the overpressure profile of the shock wave before and after its passage across the water drop curtain.

3 Experimental results

3.1 Water mist characteristics

3.1.1 Nozzle flow

The flow of each nozzle for the three nozzle types was measured (Table 2). The flow of the small-droplet nozzles (“147” and “143”) was compared to the flow of the large-droplet nozzles. The mean flow of the “147” nozzles was 14.8 lpm. This measured value was consistent with the theoretical flow of the nozzle Q (17.64 lpm) that can be obtained from the pressure and the nozzle discharge coefficient K ($Q = K\sqrt{P} = nk_v\sqrt{P}$, with n being the number of holes, k_v the hole discharge coefficient, and P the pressure in bar). The flow of the “143” nozzles was somewhat lower, at around 9 lpm. This is due to the smaller number of holes in the “143” nozzle. This measured value was below the theoretical flow of the nozzle (15.12 lpm). The mean flow of the “17” nozzles was 17.8 lpm. This value was not consistent with the theoretical flow of the nozzle (56.41 lpm) at a pressure of 120 bars.

Table 2 Measured nozzle flows under steady pump operation conditions. lpm: litres per minute

Small droplets	Flow (lpm)	Large droplets	Flow (lpm)
Nozzle 1 (F500.147.37.04)	15.6	Nozzle 1 (17)	17.0
Nozzle 2 (F500.147.37.04)	16.2	Nozzle 2 (17)	17.4
Nozzle 3 (F500.147.37.04)	16.0	Nozzle 3 (17)	17.7
Nozzle 4 (F500.147.37.04)	13.9	Nozzle 4 (17)	18.0
Nozzle 5 (F500.147.37.04)	13.0	Nozzle 5 (17)	18.2
Nozzle 6 (F500.143.37.04)	8.1	Nozzle 6 (17)	18.3
Nozzle 7 (F500.147.37.04)	14.4	Nozzle 7 (17)	17.6
Nozzle 8 (F500.143.37.04)	9.5	Nozzle 8 (17)	18.2
Mean (F500.147.37.04)	14.8	Mean	17.8
Total	106.5	Total	142.2

3.1.2 Water distribution on the floor

Figure 5 (left) presents the water distribution on the floor obtained with eight nozzles ejecting small droplets after 60 s of misting. The water distribution displayed two prominent cones corresponding to the two “143” nozzles. The

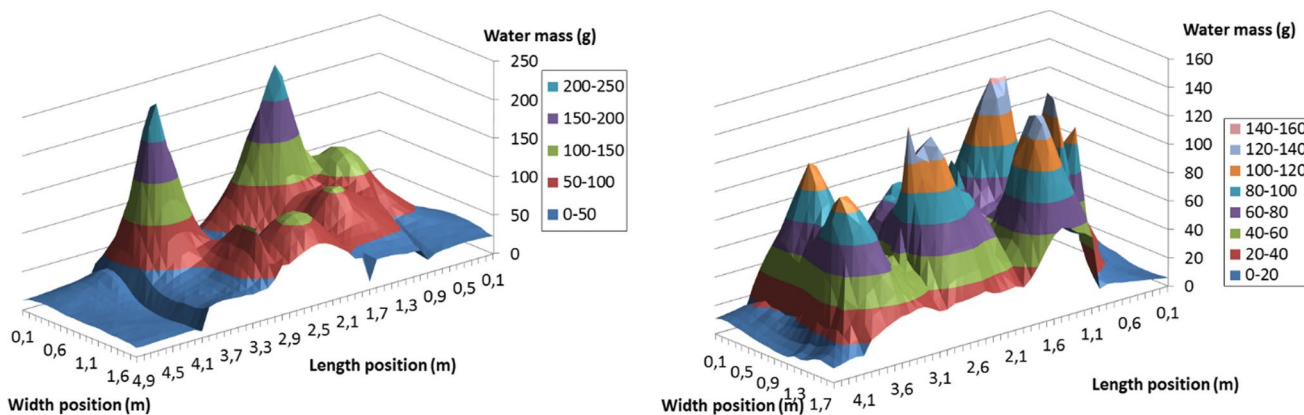


Fig. 5 Water distribution on the floor obtained with eight nozzles ejecting small droplets after 60 s of misting (left). Water distribution on the floor obtained with eight nozzles ejecting large droplets after 30 s of misting (right)

position of the holes on this type of nozzle explains why the spray jets were more oriented towards the ground and consequently why the cones were sharper. The eight nozzles were relatively close to one another. Therefore, the spray jets interacted with one another and overlapped, particularly for the type “147” nozzles. The maximum quantity of water in a box was about 106–247 g. The total quantity of water ejected during 60 s was computed and amounted to about 32 kg; this value differed by 75 kg from the total theoretical quantity of water (107 kg). The total theoretical quantity of water was calculated on the basis of each nozzle’s flow rate. Approximately, one-third of the theoretical quantity of water was not collected in the plastic boxes, and this was probably due to the water running off the walls. Some water was also found at the bottom of the pluviometer container as the plastic boxes did not fit tightly. In addition to the water running off the walls, these very small and volatile droplets were pushed outside and escaped from the tunnel.

Figure 5 (right) shows the water distribution on the floor obtained with eight nozzles ejecting large droplets after 30 s of misting. The position of the holes on this type of nozzle explains why the spray jets were more oriented towards the ground. Consequently, the cones were sharper, and there was less interference between the spray jets. The maximum quantity of water in a box amounted to about 86–144 g. The total quantity of water ejected in 30 s was about 48 kg, and this value differed by 23 kg from the total theoretical quantity of water (71 kg). The difference between the total quantity of water ejected and the total theoretical quantity of water was less marked for the nozzles producing large droplets. First, the droplets were more directed at the ground and the water runoff was reduced. Secondly, the droplets were larger and fewer droplets escaped.

3.1.3 Estimation of the water load

The water load in the tunnel could be estimated from the water distribution on the floor and from the TOF of the droplets from top to bottom in the tunnel. The water distribution gives the quantity of droplets/water that reach the floor (unit: surface of one box that is 100 cm²) over a certain period of time. The droplets, which are present in a square column the same height as the tunnel and with the surface of one of the pluviometer’s plastic boxes, contribute to the water load in this volume only during a period of time equivalent to the TOF. Consequently, the water load corresponds to the quantity of water that falls on the floor per unit of time multiplied by the TOF. The following approximations were made: a droplet rapidly reaches a position where it starts to fall and the initial velocity of the droplets has the same direction as the weight. It is thus necessary to estimate the fall of one droplet produced at altitude 0 with an initial velocity v_0 and travelling approximately 2.7 m. The droplet is modelled as a sphere. The three forces that are applied are the gravity force, the upward buoyant force, and the drag force. The drag force that is applied to a sphere of radius R that moves with a velocity of \vec{v} in the air is $\vec{F}_R = f\vec{v} = 6\pi\mu R\vec{v}$, with f being the coefficient of fluid friction of a sphere of radius R travelling in the air (μ is the viscosity coefficient of air). Whatever the radius of the sphere, the upward buoyant force can always be neglected, compared to the gravity and the drag forces. The velocity and the altitude of the drop as a function of time are derived from Newton’s second law:

$$\vec{P} + \vec{F}_R = m \frac{d\vec{v}}{dt},$$

where \vec{P} is the gravity force and m is the mass of the droplet.

That becomes:

$$mg - fv = m \frac{dv}{dt}.$$

The velocity results from solving the following equation:

$$\frac{dv}{dt} + \frac{f}{m}v - g = 0,$$

which results in

$$v(t) = \frac{gm}{f} \left(1 - \exp\left(-\frac{f \cdot t}{m}\right) \right) + v_0.$$

The integration of this equation yields the altitude. The altitude x is expressed versus time, as a function of the initial velocity of the drop v_0 and radius R as follows:

$$x(t) = -\frac{2\rho R^2}{9\mu} \left(v_0 - \frac{g \cdot 2\rho R^2}{9\mu} \right) \left(\exp\left(-\frac{9\mu \cdot t}{2\rho R^2}\right) - 1 \right) + \frac{g \cdot 2\rho R^2}{f \cdot 9\mu} t.$$

As the initial velocity was not known, the TOF was computed with v_0 equal to 0, 5, and 10 m/s for a sphere radius from 5 to 500 μm . These velocity values were chosen on the basis of measurements of mean vertical velocity performed by the manufacturer of the nozzles. It was observed that the increase in the initial velocity influences the TOF only for droplets with a radius of more than 75–100 μm and consequently, the estimation of the water load is severely affected only in this droplet size range.

For nozzles producing small droplets, if we consider the values obtained by the manufacturer, the droplet radius is around 50 μm and consequently, the TOF is around 8–9 s. The mean water load is computed for v_0 equal to 0, 5, and 10 m/s, and it ranges between 300 and 340 g/m^3 . The “17” type nozzles eject droplets with a radius around 200 μm , and consequently, the TOF ranges approximately from 1.4 to 2.4 s. The water load is lower, by about 95 to 160 g/m^3 .

3.2 Detonation tests

3.2.1 Overpressure

Supplementary Fig. 1 and Fig. 2 show the overpressure and the impulse as a function of time for three tests conducted inside the open tunnel obtained with the Gauges 1 and 5, respectively. One detonation test was conducted in air, and the other two were performed in small and large droplets. The reduction in the overpressure and of the impulse by the water mist is observable. Table 3 presents the mean initial overpressure for the experiments conducted in air and in small and large droplets, obtained with Gauges 1, 2, 3, 4, and 5, in the open tunnel. The measurement reproducibility was rather good, and the values obtained with Gauge 3 and Gauge 4, which are symmetrical, were comparable. The initial overpressure was reduced by the presence of the water mist, and this was noticed on all the gauges. The reduction was about 34–50% for large droplets and about 32–42% for small droplets. The reduction was comparable for both droplet sizes.

Supplementary Fig. 3 presents the overpressure and the impulse as a function of time for three tests conducted inside the closed tunnel obtained with the Gauge 1. One test was performed in air, and the other two were carried out in small and large droplets. The attenuation of the overpressure and of the impulse by the water mist is clearly visible. Table 4 presents the mean initial overpressure for the experiments conducted in air and in small and large droplets, obtained with Gauges 1, 2, 3, and 4, in the closed tunnel. The intensity of the first additional peak in overpressure, due to shock wave reflections within the closed tunnel, is also given. The standard deviation was not computed for the series of measurements, while the number of tests was not sufficient (less than six). Nevertheless, the examination of the different values showed a good reproducibility. The overpressure

Table 3 Mean initial overpressure for the experiments conducted in air and in small and large droplets, obtained with Gauges 1, 2, 3, 4, and 5, in the open tunnel

Type of test	Initial overpressure (bar)				
	Gauge no. (distance to the charge)				
	Gauge 1 (1.59 m)	Gauge 2 (1.02 m)	Gauge 3 (1.24 m)	Gauge 4 (1.24 m)	Gauge 5 (2.10 m)
Air	1.32	3.17	2.05	1.92	0.30
SD	0.10	0.20	0.07	0.17	0.01
Large	0.79	2.08	1.02	1.07	0.20
SD	0.07	0.24	0.16	0.21	0.02
Percentage difference to air	−40	−34	−50	−44	−35
Small	0.87	2.14	1.38	1.12	0.21
SD	0.04	0.33	0.18	0.16	0.01
Percentage difference to air	−34	−32	−33	−42	−30

The standard deviation (SD) and the percentage difference between the values obtained with air and with the two sizes of droplets are also given

Table 4 Mean initial overpressure of the first and the second peak for the experiments conducted in air and in small and large droplets, obtained with Gauges 1, 2, 3, and 4, in the closed tunnel

Type of test	Initial overpressure (bar)							
	Gauge no. (distance to the charge)							
	Gauge 1 (1.59 m)		Gauge 2 (1.02 m)		Gauge 3 (1.24 m)		Gauge 4 (1.24 m)	
	Initial	Second peak	Initial	Second peak	Initial	Second peak	Initial	Second peak
Air	1.43	0.82	3.42	0.99	2.13	0.92	2.10	1.05
Large	1.06	0.64	2.43	0.34	1.27	0.53	1.40	0.59
Percentage difference to air	-26	-22	-29	-66	-41	-42	-33	-43
Small	1.06	0.59	2.40	0.32	1.46	0.66	1.26	0.62
Percentage difference to air	-26	-28	-30	-67	-32	-28	-40	-40

The standard deviation (SD) and the percentage difference between the values obtained with air and with the two sizes of droplets are also given

values were reduced by the presence of the water mist, and this can be observed on all the gauges. The reduction ranged between 22 and 66% for large droplets and about 26–67% for small droplets. The reduction was comparable for both droplet sizes. It could be noted that the attenuation of the first additional peak in overpressure due to shock wave reflections was not higher than the one achieved for the initial overpressure peak for the Gauges 1, 3, and 4, but it was higher for the Gauge 2. It is somewhat difficult to state if this is meaningful.

Supplementary Fig. 4 and Fig. 5 show the overpressure and the impulse as a function of time for three tests performed outside the tunnel obtained with the Gauges 1 and 5, respectively. One detonation test was conducted in air, and the other two were performed in small and large droplets. The initial overpressure was reduced by the presence of the mist for the Gauge 1 located on the tunnel wall, and a slight decrease in the maximum impulse could be observed (Supplementary Fig. 4). But for the Gauge 5 placed at the end of the tunnel, the reduction is not obvious (Supplementary

Fig. 5). Table 5 presents the mean initial overpressure for the experiments conducted in air and in small and large droplets, obtained with Gauges 1, 2, 3, 4, and 5, when the charge detonated in front of the tunnel. Two positions for Gauge 5 were tested, either at the end of the tunnel in the middle or at the end of the tunnel off-centre to be aligned with one line of nozzles. These two positions allow the assessment of the effect of the water mist amount on the blast wave path. Indeed, the mist is probably denser just below the nozzles. The initial overpressure was reduced for the five gauges but to a much lesser extent than when the charges were detonated inside the mist. The overpressure reduction was about 20% for the gauges located on the tunnel walls, but for the Gauge 5, no significant attenuation was observed whatever the position of the gauge. There was no more effect on the overpressure when the Gauge 5 was aligned with one line of nozzles. Although the mist should be more dense just below the nozzles and there was probably more amount of mist on the blast wave path, the overpressure was not more affected than when the gauge was located in the middle, at

Table 5 Mean initial overpressure for the experiments conducted in air and in small and large droplets, obtained with Gauges 1, 2, 3, 4, and 5, when the charge detonated in front of the tunnel

Type of test	Initial overpressure (bar)					
	Gauge no. (distance to the charge)					
	Gauge 1 (5 m)	Gauge 2 (6 m)	Gauge 3 (7 m)	Gauge 4 (7 m)	Gauge 5 (8.6 m)	Gauge 5 (9 m)
Air	1.24	0.90	0.75	0.81	0.55	0.44
SD	0.06	0.01	0.04	0.01	–	–
Large	0.94	0.71	0.58	0.63	0.50	0.47
SD	0.06	0.05	0.03	0.03	–	–
Percentage difference to air	-24	-21	-22	-22	-9	6
Small	0.94	0.80	0.58	0.64	–	0.44
Percentage difference to air	-24	-11	-23	-20	–	-1

The standard deviation (SD) (when the number of experiments is higher or equal to 6) and the difference between the values obtained with air and with the two sizes of droplets are also given

equal distance from the two nozzle lines. The results were comparable for both droplet sizes. It could be noted that the reproducibility was good.

In the case of the closed tunnel, the effect of the mist on the quasi-static pressure was examined. The quasi-static pressure was computed as follows: after the initial blast overpressure, the pressure returns near/below zero before distinctly rising again and this corresponds to the start of the quasi-static pressure region (t_0); a value was calculated for two different time periods (δt), 0.01 and 0.05 s. The quasi-static value corresponds to the impulse between t_0 and $t_0 + \delta t$ divided by δt . Table 6 presents the means of two quasi-static pressure values computed for the tests conducted in air and in small and large droplets. The percentage reduction compared to the quasi-static pressure values obtained with air is also given. For both droplet sizes, the quasi-static pressure was strongly reduced by the presence of water mist.

3.2.2 Time of arrival

The supplementary Table 2 presents the time of arrival (ToA) of the initial overpressure obtained with Gauges 1, 2, 3, 4, and 5, averaged for each type of tests (air, small, or large droplets), for all detonations conducted inside the tunnel (open or closed). The reproducibility was rather good. As expected, the ToA increased with the distance to the charge. Moreover, the shock wave was delayed by the presence of the mist, and this delay increased with the distance from the charge and consequently with the amount of mist the shock wave passed through.

The supplementary Table 3 presents the ToA of the initial overpressure obtained with Gauges 1, 2, 3, 4, and 5, averaged for each type of tests for all detonations conducted in front of the tunnel. The reproducibility was very good. As expected, the ToA increased with the distance to the charge. The increase in ToA in the mist compared to air was not obvious, only on the Gauge 5 located at the farther distance.

3.2.3 Impulse

Table 7 presents the maximum impulse averaged for each type of tests (air, small, or large droplets) for the detonations conducted inside the tunnel obtained with Gauges 1, 2, 3, 4, and 5. The impulse corresponds to the overpressure signal integrated over time. The measurements were very reproducible. When the charge detonated inside the open tunnel, the impulse was reduced by the presence of the water mist, and this was visible on the five gauges. The reduction was about 30–41% for large droplets and about 26–35% for small droplets. The reduction was in the same range for both droplet sizes. It could be noted that the impulse decrease was a consequence of the corresponding overpressure decrease measured by the pressure gauge. The contribution to impulse of the impact of the droplets or of droplet fragments could not be obtained by this way and consequently was not taken into account. Similarly, the maximum impulse was reduced by the presence of the water mist when the tunnel was closed and this was visible on the four gauges. The attenuation was equivalent for the both droplet sizes, and it ranged around 30%.

Table 8 presents the maximum impulse averaged for each type of tests (air, small, or large droplets) for the detonations conducted in front of the tunnel obtained with Gauges 1, 2, 3, 4, and 5. The reproducibility of this experiment was very good. The impulse was not reduced significantly by the presence of the water mist, and this was observed on the five gauges. The same result was obtained for both droplet sizes.

3.3 Shock tube experiments

Figure 6 presents the different stages in the deformation and break-up of a water drop (1.91 mm in diameter) in the flow behind a Mach 1.3 shock wave. Other experiments with several droplet sizes (from 0.62 to 1.91 mm) led to the same observations. Pictures were taken at 45,000 fps (time

Table 6 Means of two quasi-static pressure values computed for the tests conducted in air and in small and large droplets

Type of test	Quasi-static pressure (bar)							
	Gauge no. (distance to the charge)							
	Gauge 1 (1.59 m)		Gauge 2 (1.02 m)		Gauge 3 (1.24 m)		Gauge 4 (1.24 m)	
	QS 0.01	QS 0.05	QS 0.01	QS 0.05	QS 0.01	QS 0.05	QS 0.01	QS 0.05
Air	0.187	0.039	0.199	0.103	0.145	-0.026	0.120	0.038
Large	0.068	0.004	0.029	-0.015	0.042	0.001	0.045	0.002
Percentage difference to air	-64	-89	-86	-114	-71	-104	-63	-96
Small	0.080	0.008	0.062	0.012	0.061	0.014	0.063	0.013
Percentage difference to air	-57	-80	-69	-89	-58	-153	-47	-67

The percentage reduction compared to the quasi-static values obtained with air. QS 0.01: quasi-static pressure calculated on a time period of 0.01 s. QS 0.05: quasi-static pressure calculated on a time period of 0.05 s

Table 7 Maximum impulse averaged for each type of tests (air, small, or large droplets) for the detonations conducted inside the tunnel obtained with Gauges 1, 2, 3, 4, and 5

Type of test (test no.)	Maximum impulse (bar-s)				
	Gauge no. (distance to the charge)				
	Gauge 1 (1.59 m)	Gauge 2 (1.02 m)	Gauge 3 (1.24 m)	Gauge 4 (1.24 m)	Gauge 5 (2.10 m)
Air—open tunnel	0.00038	0.00066	0.00058	0.00055	0.00013
SD	0.00002	0.00002	0.00004	0.00002	0.00001
Large—open tunnel	0.00025	0.00046	0.00034	0.00035	0.000094
SD	0.00002	0.00002	0.00002	0.00001	0.000003
Percentage difference to air	-33	-30	-41	-36	-30
Small—open tunnel	0.00027	0.00049	0.00038	0.00037	0.000097
SD	0.00001	0.00006	0.00002	0.00001	0.000004
Percentage difference to air	-28	-26	-35	-32	-27
Air—closed tunnel	0.00039	0.00071	0.00059	0.00055	-
Large—closed tunnel	0.00027	0.00052	0.00038	0.00038	-
Percentage difference to air	-31	-26	-36	-32	-
Small—closed tunnel	0.00030	0.00056	0.00043	0.00039	-
Percentage difference to air	-23	-21	-28	-29	-

The standard deviation (SD) and the difference between the mean values obtained with air and with the two sizes of droplets are also given

Table 8 Maximum impulse averaged for each type of tests for the detonations conducted in front of the tunnel, obtained with Gauges 1, 2, 3, 4, and 5

Type of test	Maximum impulse (bar-s)					
	Gauge no. (distance to the charge)					
	Gauge 1 (5 m)	Gauge 2 (6 m)	Gauge 3 (7 m)	Gauge 4 (7 m)	Gauge 5 (8.6 m)	Gauge 5 (9 m)
Air	0.0019	0.00183	0.0019	0.00198	0.0019	0.0011
SD	0.0001	0.00004	0.0001	0.00004	-	-
Large	0.0018	0.00181	0.0019	0.0019	0.0017	0.0011
SD	0.0001	0.00004	0.0001	0.0001	-	-
Percentage difference to air	-3	-1	-1	-3	-6	-3
Small	0.0017	0.0018	0.0018	0.0019	-	0.0011
Percentage difference to air	-8	-4	-7	-4	-	-3

The standard deviation (SD) (when the number of experiments is higher or equal to 6) and the difference between the mean values obtained with air and with the two sizes of droplets are also given

interval 22 μs) with a resolution of 1024 × 256 pixels. A pixel on the picture represents a real distance of 0.063 mm.

The fluid dynamics of compressed hot gas behind the shock after it has passed over the drop is the disturbing factor responsible for drop fragmentation. The passage of the shock over the drop has no significant impact on break-up. Forty-four microseconds after the shock wave has passed the drop, it begins to deform. On the drop side behind the shock front, the drop flattens, and on the opposite side, the outward water layer flows from the edge of the drop to its equator. The boundary layer is stripped, and the water accumulates at the equator. After 88 μs, the liquid accumulated on the equator starts to be blown off. Thereafter, the drop takes a lenticular shape, i.e., the

front is hemispherical and the back is flat. The lenticular drop shape stems from the fact that the flow of liquid is dragged around the nose and accumulated on the equator of the drop. Afterwards, drop fragmentation continues, the lenticular drop disintegrates, and the break-up produces ultrafine droplets. The core of the droplet persists for a long time; after 946 μs, it is still visible.

In order to assess the effects of water droplets on the shock wave profile, experiments were conducted with a water drop curtain. Direct visualisation was used with higher magnification so that a pixel on the picture corresponds to a real distance of 0.066 mm. The drop diameter is about 2 mm. Figure 7 shows the passage of the shock wave across the water droplets and the fragmentation of

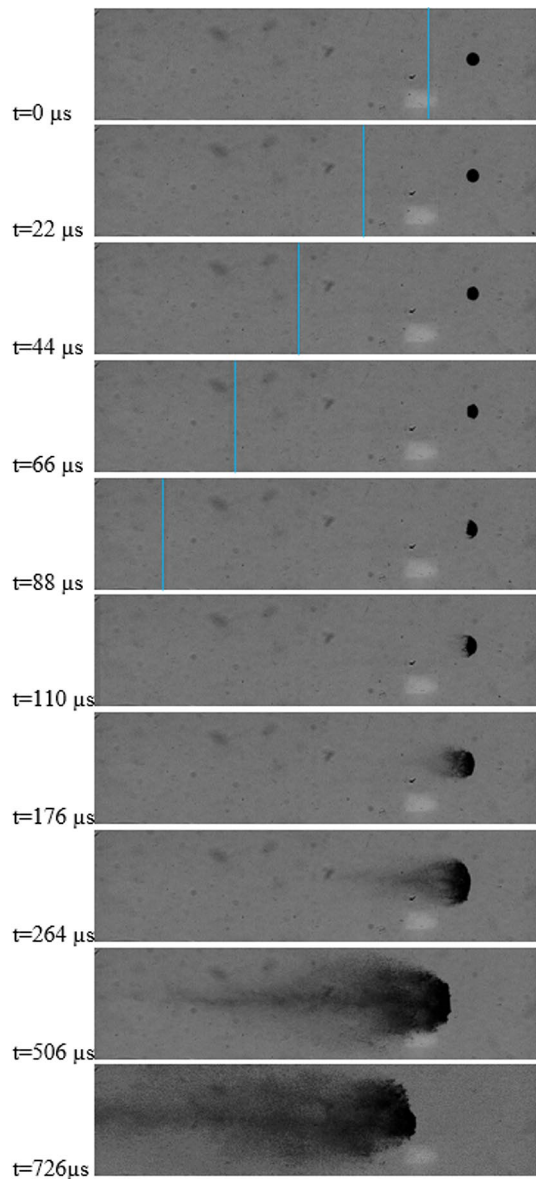


Fig. 6 Stages in the deformation and break-up of a water drop (1.91 mm in diameter) in the flow behind a Mach 1.3 shock wave; $t=0 \mu\text{s}$ corresponds to the first image where the shock wave has passed the drop. The shock front is indicated by a blue line

the droplets. Figures 8 and 9 show the pressure profiles versus time obtained with the gauges positioned upstream (Gauge 1) and downstream (Gauge 2) from the water drop curtain, respectively. We observed that the water droplets had no effect on the shock wave pressure profile.

4 Discussion

In this work, it was observed that the nozzles generating small droplets maintained a pump pressure of 120 bars. The measured flow was consistent with the theoretical flow of the nozzle that can be obtained from pressure and nozzle discharge coefficient k_v . This was not the case for the nozzles generating large droplets, and the flow was much lower than the theoretical flow. The pressure/flow has an impact on the ejected droplet size, and the droplet size becomes smaller when the pressure increases. As a result, we cannot exclude that the large droplets were a little bit larger than the theoretical size given by the manufacturer, that is, 200–300 μm . Consequently, the assessment of the droplet size effect, independent of the mist concentration effect, on mitigation efficiency is not so simple. It is not easy to change independently these mist parameters using a firefighting system. Willauer and co-authors [12] encountered the same issue. With their water mist system, they were able to produce different mist concentrations by reducing the pump pressure, but different droplet size resulted.

According to our results, the mitigation efficiency was similar for both droplet sizes, but it should be taken into account that the water mist density was different. We obtained a smaller mist density with nozzles ejecting large droplets, and the mitigation efficiency was equivalent. We can assume that droplets with a diameter of 200–300 μm are more effective in attenuating the blast produced by a high explosive. This observation needs to be confirmed. Willauer et al. [12] obtained a comparable reduction for two different droplet sizes (SMD of 54 μm and 83 μm), but the charge mass used was different. Opposite views on the droplet size effect were formulated. Thomas [5] proposed that large droplets (> 1 mm) with large inertia could be more effective than small droplets, but numerical computations showed [19] that the absorption of the latent heat of vaporisation is the dominant mechanism of energy absorption, and thus, small droplets could contribute more effectively to the energy extraction as their vaporisation duration is shorter. However, it was not excluded that large droplets could fragment and although the fragmentation energy is low compared to the vaporisation energy of water, the fragmentation could be necessary for the global process. Small droplets are generated and these could evaporate rapidly.

Concerning the water load estimation, we obtain much higher values than those published in the literature. These values were most often estimated, and the estimation method was not given. In the previous published studies, the water flows used were also much lower than ours: 3 lpm for one nozzle [14]; 6 lpm for one nozzle [10]. We have seen here that the quantity of water in a mist calculated on the basis of a nozzle's flow rate was largely overestimated, and this was

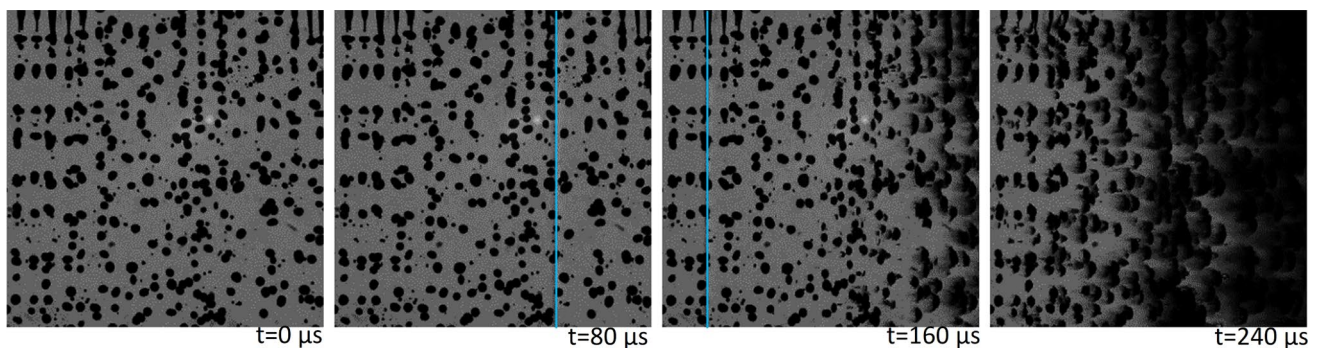


Fig. 7 Photographs showing the passage of the shock wave across the water droplets and the fragmentation of the droplets in the case of a water drop curtain. The shock front is indicated by a blue line. At the initial time of 0 μs , the shock has not processed the drops

Fig. 8 Pressure profile versus time obtained with the gauge upstream from the water drop curtain in experiments with a water drop curtain

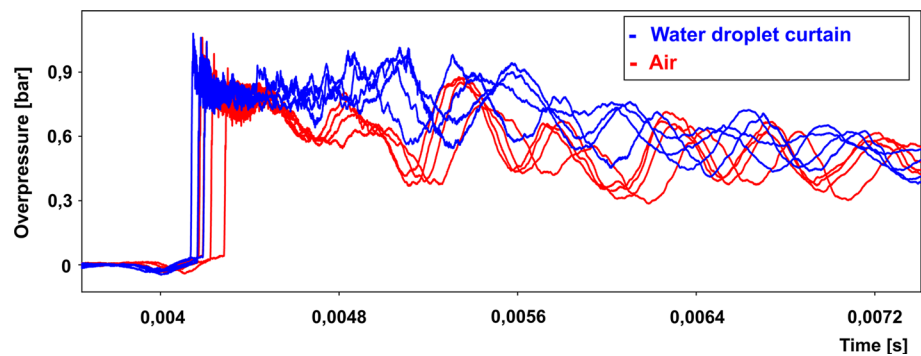
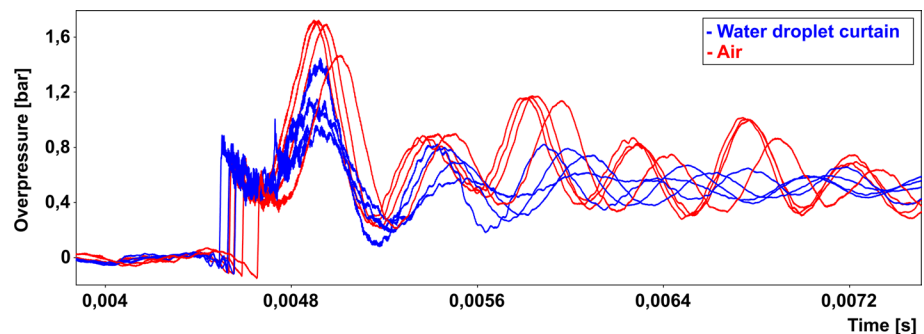


Fig. 9 Pressure profile versus time obtained with the gauge downstream from the water drop curtain in experiments with a water drop curtain



probably due to the water running off the walls. In only one study [11, 12], laser diffraction measurements were realised and the measured water load ranged between 29 and 87 g/cm^3 and SMD of droplets from 30 to 85 μm . The flow rate was also rather high (74 to 170 lpm). At first, we also envisaged to measure the droplet size distribution and the water load of the mists by laser diffraction, but unfortunately, the results were not satisfying. First, the outdoor brightness interfered with the calibration of the device, and secondly, the mists were so dense that the particle size analyser was rapidly saturated. We could make the assumption that the water load evaluation method used here overestimated the mist amount. This could be attributed to the TOF estimation. The TOF for droplets with a radius of more than 75–100 μm

depends strongly on their initial velocity. Consequently, the water load estimation could be biased for these droplet sizes.

The shock wave was delayed by the presence of the mist, and this delay increased with the distance to the charge and thus with the quantity of water mist the shock wave passed through. This observation could be expected as the water droplets probably acted as a barrier standing in the way of the blast wave. Bailey et al. [9] also noticed that the presence of water mist delayed the beginning of the initial blast overpressure waves. For three different TNT charge masses (0.9, 2.2, and 3.2 kg), the maximum reduction in start time was never more than 0.0005 s. In their work, the shock wave path in the mist was around 3.25 m. When the charge detonated inside the mist, we obtained a delay of 0.00031 s for a

shock wave path in the mist of 2.10 m. When the detonation occurred outside the mist, the shock wave path in the mist ranged between 1 and 5 m and the reduction in TOA ranged between 0.00004 and 0.0010 s. These values were consistent and indicated that the shock wave delay increases with the quantity of mist on the shock wave path, although the detonation location appeared to affect this delay.

Regarding the effects of the water mist on blast, the initial overpressure reduction by the presence of the mist ranged between 26 and 50% depending on the gauge location when the charge detonated inside the mist. When the explosion was initiated outside the mist, the reduction ranged just between 10 and 24%. The maximum impulse was only reduced by the mist when the explosion was inside the mist (21 to 41%, depending on the gauge location). Resnyansky and Delaney [10] obtained a reduction of 10% in overpressure with charges of 500 g of Composition B. The droplet diameters were in the same range (50–100 μm) as those of our small droplets, but the quantity of mist around the charge was much smaller. They used four nozzles located above the charge, separated by 1 m, and the flow of one nozzle was only 6 lpm. The pressure gauges were located outside the mist. In the present work, eight nozzles having a much higher flow were used. Thus, the difference of efficiency is probably due to the smaller mist concentration. With a configuration in which the mist was generated by a line of three nozzles positioned 1 m behind the charge, the overpressure reduction, measured inside the mist, was in the same range as ours (20%). The amount of mist on the blast path was more comparable. Indeed, although the nozzle flow was lower, the blast was affected by three nozzles ejecting droplets on a distance of 2 m. In our case, the blast wave impacted a mist generated by four nozzles placed at a distance of 3.375 m. Willauer et al. [11, 12] assessed the blast mitigation generated by 22.7 kg of TNT and by a Destex and a PBXN-109 charge having the same TNT equivalent, with a configuration of nozzles similar to ours. The droplet size was comparable, but the mist concentration was somewhat lower, 70 g/m^3 , but nonetheless fairly high. The impulse and initial blast wave overpressure for the TNT charge were reduced by 40% and 36%, respectively. For the Destex charge, the reduction in initial overpressure was somewhat lower (25%), but the reduction in impulse was equivalent (43%). The quasi-static overpressure reduction was similar for both charges: it ranged between 33 and 35%. For the PBXN-109 charge, the impulse, initial blast wave, and quasi-static overpressure were reduced by 49%, 39%, and 41%. It could be noted that although these three explosives (one conventional and two thermobaric explosives) had different behaviour, the attenuations were in the same range. Another study [15] has assessed the water mist mitigation of 10 g of RDX that exploded outside the mist. Three water loads were assessed: 5.1 g/m^3 , 19.8 g/m^3 , and 36.6 g/m^3 , and the overpressure was

reduced by 22%, 47%, and 53%, respectively. These rather high-pressure reductions are rather surprising but could be attributed to the fact that the mass–charge was very small. Overall, the amount of mitigation provided by the water mist in this study is consistent with previous investigations.

Concerning the effects of detonation location on the blast mitigation efficiency, the initial overpressure was greatly reduced by the presence of the mist when the charge detonated in the mist. The initial overpressure was slightly modified when the explosion occurred outside the mist. In the same way, the impulse was only strongly reduced when the charge detonated inside the mist. Thanks to the shock tube experiments, we have observed that the water droplets accelerated and broke up in the high-speed airstream behind the shock wave long after the shock wave passage. Moreover, the shock wave profile was almost not modified by the presence of the water droplet curtain. In the literature, it was proposed that some energy is extracted from the blast wave for droplet acceleration, fragmentation, and vaporisation. The quenching of secondary reactions has also been considered as a mechanism leading to blast mitigation by water mist. According to our results, we could assume that droplet acceleration and break-up does not play an important role in explosion mitigation and that the blast mitigation is probably mostly due to the extinguishment of the fireball. This hypothesis could be supported with results from studies dealing with the interaction of a shock wave with bulk water. It has been shown that when a detonating charge is surrounded by a large amount of water, the overpressure is strongly reduced. If the water is placed to a certain distance, the attenuation is much lower [3]. Chen et al. [4] assessed blast mitigation using water walls, and they claimed that the mitigation arises from the obstruction, the reflection, and the diffraction of the blast wave by the water wall and the mitigation mechanism is comparable to that of a rigid wall. The comparison with a rigid wall proved that the mitigation effects of energy exchange with water are not the major effects and only a part of blast wave energy was transformed into kinetic energy of droplets. Gebbeken et al. [20] tested a mitigation solution made of a stainless steel ring mesh in combination with a flowing water layer. They also claimed that when the blast wave hits the ring mesh covered by water, the water layer forms a closed surface which reflects more the blast wave. The mitigation of a blast wave after its passage through a perforated plate or a chain mail covered or not by a water film was also assessed [21]. With the help of experiments in a shock tube, it was observed that the water film disintegrated into droplets long after the passage of the shock wave front. It has been proposed that the water layer contributed mostly to enhance the reflection of the shock wave, and it is likely that the fragmentation of the water film had little effect on the attenuation as it broke long after the shock wave front passage. The extraction of energy from

the shock front for water layer fragmentation was probably small.

5 Conclusions

The aim of this research was to assess the mitigation of an explosion by water mist generated by a water mist fire suppression system in three detonation scenarios. The charge was detonated either inside the mist (the tunnel could be closed or open) or in front of the mist. We also attempted to study the mitigation efficiency as a function of the droplet size. It has been shown that it is not easy to change independently the droplet size and the mist concentration using a firefighting system. Consequently, the assessment of the droplet size effect, independent of the mist concentration effect, on mitigation efficiency was not really possible. According to our results, the mitigation efficiency was similar for both droplet sizes, but the water mist density was different. With nozzles ejecting large droplets, mist density was smaller. Concerning the effects of detonation location on the blast mitigation efficiency, the initial overpressure and maximum impulse were only greatly reduced by the presence of the mist when the charge detonated in the mist. Thanks to the shock tube experiments, we observed that the water droplets accelerated and broke up in the high-speed airstream behind the shock wave long after the shock wave passage. The results obtained here support the fact that droplet acceleration and break-up does not play an important role in explosion mitigation and that the blast mitigation is probably mostly due to the extinguishment of the fireball and the quenching of the secondary reactions.

Acknowledgements We thank our colleagues Thierry Ottié and Eric Schmitt who assisted us in our research by providing technical support.

Compliance with ethical standards

Conflict of interest The authors declare that they have no conflict of interest.

References

- Buzukov, A.A.: Decreasing the parameters of an air shock wave using an air–water curtain. *Combust. Explos. Shock Waves* **36**, 395–404 (2000). <https://doi.org/10.1007/BF02699393>
- Pitiot, F., Chabin, P., Desailly, D.: Blast wave mitigation by water: full scale tests and numerical modelling. 29th DDESB Explosives Safety Seminar, New Orleans, LA, USA (2000)
- Forsen, R., Carlberg, A., Eriksson, S.: Small scale tests on mitigation effects of water in a model of the Klotz Club Installation in Alvdalen. 27th DoD Explosives Safety Seminar, Las Vegas, NV, USA (1996)
- Chen, L., Zhang, L., Fang, Q., Mao, Y.-M.: Performance based investigation on the construction of anti-blast water wall. *Int. J. Impact Eng* **81**, 17–33 (2015). <https://doi.org/10.1016/j.ijimpeng.2015.03.003>
- Jones, A., Thomas, G.O.: On the action of water sprays on fires and explosions: a review of experimental work. *Process Saf. Environ Prot., IChemE* **71**, 41–49 (1993)
- Tam, V.H.Y., O'Connell, M., Pedersen, G., Renwick, P.: Testing of the Micromist device: an active soft barrier for explosion control. *J. Loss Prev. Process Ind.* **16**, 81–88 (2003). [https://doi.org/10.1016/S0950-4230\(02\)00024-4](https://doi.org/10.1016/S0950-4230(02)00024-4)
- Thomas, G.O.: On the conditions required for explosion mitigation by water sprays. *Process Saf. Environ Prot., IChemE* **78**, 339–354 (2000). <https://doi.org/10.1205/095758200530862>
- Catlin, C.A., Gregory, C.A.J., Johnson, D.M., Walker, D.G.: Explosion mitigation in offshore modules by general area deluge. *Process Saf. Environ Prot., IChemE* **71**, 101–111 (1993)
- Bailey, J.L., Farley, J.P., Williams, F.W., Lindsay M.S., Schwer D.A.: Blast mitigation using water mist. NRL report, NRL/MR/6180-06-8933 (2006) <https://apps.dtic.mil/dtic/tr/fulltext/u2/a443885.pdf>
- Resnyansky, A.D., Delaney, T.G.: Experimental study of blast mitigation in a water mist. DSTO report, DSTO-TR-1944 (2006) <http://dspace.dsto.defence.gov.au/dspace/bitstream/1947/4562/1/DSTO-TR-1944.PR.pdf>
- Willauer, H.D., Ananth, R., Farley, J.P., Williams, F.W.: Mitigation of TNT and Destex explosion effects using water mist. *J. Hazard. Mater.* **165**, 1068–1073 (2009). <https://doi.org/10.1016/j.jhazmat.2008.10.130>
- Willauer, H.D., Ananth, R., Farley, J.P., Williams, F.W., Back, G.G., Kennedy, M.C., O'Connor J., Gameiro V.M.: Blast mitigation using water mist: Test series II. NRL report, NRL/MR/6180-09-9182 (2009)
- Ananth, R., Willauer, H.D., Farley, J.P., Williams, F.W.: Effects of fine water mist on a confined blast. *Fire Technol.* **48**, 641–675 (2012). <https://doi.org/10.1007/s10694-010-0156-y>
- Tosello, R., Leriche, D., Chauvin, A., Zerbib, J., Jourdan, G., Daniel, E., Mariani, C., Houas, L., Biamino, L.: Shock wave attenuation using water mist. Abstracts of the 22nd Symposium on Military Aspects of Blast and Shock, Bourges, France (2012). <https://www.mabs.ch/spiez-base/mabs-21-to-25/mabs-22/>
- Mataradze, E., Krauthammer, T., Chikhradze, N., Chagelishvili, E.: Shock energy absorber for protection of underground structure from internal explosions. 15th International Symposium on Interaction of the Effects of Munitions with Structures, Postdam, Germany (2013)
- Schwer, D.A., Kailasanath, K.: Blast mitigation by water mist (3) Mitigation of confined and unconfined blasts. NRL report, NRL/MR/6410-06-8976 (2006). <https://apps.dtic.mil/dtic/tr/fulltext/u2/a452669.pdf>
- Breda, C., Kerampran S., Sturtzer, M.-O., Arrigoni, M., Legendre, J.F.: Analysis of planar and spherical shock-wave mitigation by wet aqueous foams. In: Kontis, K. (Ed.) *Shock Wave Interactions, Selected Articles from the 22nd International Shock Interaction Symposium*, University of Glasgow, United Kingdom, 4–8 July 2016, pp. 279–297. Springer International Publishing, Cham (2018). <https://doi.org/10.1007/978-3-319-73180-3>
- Del Prete, E., Chinnayya, A., Domergue, L., Hadjadj, A., Haas, J.-F.: Blast wave mitigation by dry aqueous foams. *Shock Waves* **23**, 39–53 (2013). <https://doi.org/10.1007/s00193-012-0400-0>
- Schwer, D.A., Kailasanath, K.: Numerical simulations of the mitigation of unconfined explosions using water mist. *Proc. Combust. Inst.* **31**, 2361–2369 (2007). <https://doi.org/10.1016/j.proci.2006.07.145>

20. Gebbeken, N., Rüdiger, L., Warnstedt, P.: Explosion mitigation by water mist-ring mesh with water curtain. Abstracts of the 25th Symposium on Military Aspects of Blast and Shock, The Hague, The Netherlands (2018). <https://www.mabs.ch/spiez-base/mabs-21-to-25/mabs-25/>
21. Schunck, T., Bastide, M., Eckenfels, D., Legendre, J.-F.: Explosion mitigation by metal grid with water curtain. Proc. of the 32nd International Symposium on Shock Waves (ISSW32),

Research Publishing, Singapore, pp. 1629–1647 (2019). https://doi.org/10.3850/978-981-11-2730-4_0237-cd

Publisher's Note Springer Nature remains neutral with regard to jurisdictional claims in published maps and institutional affiliations.